AIAA Propulsion and Energy Forum
July 28-30, 2014, Cleveland, OH
50th AIAA/ASME/SAE/ASEE Joint Propulsion Conference

10.2514/6.2014-3429

Check for updates

Downloaded by University of Michigan - Duderstadt Center on December 13, 2017 | http://arc.aiaa.org | DOI: 10.2514/6.2014-3429

Influence of Triply-Charged Ions and Ionization Cross-Sections in a Hybrid-PIC Model of a Hall Thruster Discharge

Brandon D. Smith* and Iain D. Boyd†
Nonequilibrium Gas and Plasma Dynamics Laboratory
University of Michigan, Ann Arbor, Michigan, 48109, USA

and

Hani Kamhawi‡
NASA Glenn Research Center, Cleveland, Ohio, 44135, USA

The sensitivity of xenon ionization rates to collision cross-sections is studied within the framework of a hybrid-PIC model of a Hall thruster discharge. A revised curve fit based on the Drawin form is proposed and is shown to better reproduce the measured cross-sections at high electron energies, with differences in the integrated rate coefficients being on the order of 10% for electron temperatures between 20 eV and 30 eV. The revised fit is implemented into HPHall and the updated model is used to simulate NASA's HiVHAc EDU2 Hall thruster at discharge voltages of 300, 400, and 500 V. For all three operating points, the revised cross-sections result in an increase in the predicted thrust and anode efficiency, reducing the error relative to experimental performance measurements. Electron temperature and ionization reaction rates are shown to follow the trends expected based on the integrated rate coefficients. The effects of triply-charged xenon are also assessed. The predicted thruster performance is found to have little or no dependence on the presence of triply-charged ions. The fraction of ion current carried by triply-charged ions is found to be on the order of 1% and increases slightly with increasing discharge voltage. The reaction rates for the 0→III, I→III, and II→III ionization reactions are found to be of similar order of magnitude and are about one order of magnitude smaller than the rate of 0→II ionization in the discharge channel.

Nomenclature

EDU2	Engineering development unit 2	
EEDF	Electron energy distribution function	
GRC	Glenn Research Center	
HiVHAc	High Voltage Hall Accelerator	
PIC	Particle-in-cell	
α_a	Bohm coefficient for region a	
β_k	kth fitting coefficient for Drawin curve fit	
ϵ_e	Electron energy	eV
ϵ_i	Ionization energy for a given reaction	eV
ϵ_i^H	Ionization energy of hydrogen	eV
η_a	Thrust-derived anode efficiency	
λ	Magnetic stream function	$\mathrm{T{\cdot}m^2}$

*Ph.D. Candidate, Department of Aerospace Engineering, bradenis@umich.edu, AIAA Student Member.
†James E. Knott Professor, Department of Aerospace Engineering, iainboyd@umich.edu, AIAA Fellow.
‡Research Engineer, In-Space Propulsion Systems, hani.kamhawi-1@nasa.gov, AIAA Associate Fellow.

Copyright © 2014 by the American Institute of Aeronautics and Astronautics, Inc.
All rights reserved.

$\mu_{e,\perp}$	Electron cross-field mobility	$m^2/V{\cdot}s$
ν_e	Total effective electron collision frequency	s^{-1}
ν_b	Anomalous Bohm collision frequency	s^{-1}
ν_{ei}	Electron-ion collision frequency	s^{-1}
ν_{en}	Electron-neutral collision frequency	s^{-1}
ν_w	Effective wall collision frequency for electrons	s^{-1}
Ω_e	Electron Hall parameter	
ϕ, ϕ^*	Local and thermalized plasma potential	V
σ_i	Collision cross-section for a given ionization reaction	m^2
ξ	Number of equivalent electrons in valence subshell	
ζ	Reaction rate coefficient	m^3/s
a_0	Bohr radius	m
B	Magnetic field	T
e	Elementary charge	C
f_e	Electron energy distribution function	eV^{-1}
F_{th}	Thrust force	N
I_b	Total ion beam current	A
I_b^{Z+}	Current carried by ions of charge state Z	A
I_d	Discharge current	A
I_{sp}	Anode specific impulse	s
k_B	Boltzmann constant	J/eV
$\dot{m}_a$	Anode mass flow rate	kg/s
m_e	Electron mass	kg
$n_e, n_{e,0}$	Local and reference electron density	m^{-3}
n_i	Total ion number density	m^{-3}
n_n	Neutral atom number density	m^{-3}
n_i^{Z+}	Number density of ions with charge state Z	m^{-3}
p_c	Operating chamber pressure measured at thruster location, corrected for xenon	Torr
$\Delta t_e, \Delta t_i$	Electron and ion time steps	s
T_e	Electron temperature	eV
V_d	Discharge voltage	V

Downloaded by University of Michigan - Duderstadt Center on December 13, 2017 | http://arc.aiaa.org | DOI: 10.2514/6.2014-3429

I. Introduction

Hall effect thrusters (HETs) are an attractive technology for in-space propulsion due to their relatively high specific-impulse and ratio of thrust-to-power. However, there are many physical processes in Hall thrusters that are still poorly understood, such as the rate of sputter erosion of the discharge channel walls and the unexpectedly high mobility of electrons across magnetic field lines. Experimental insight into these problems has been limited due to a lack of adequate measurement techniques, and the coupled nature of the governing equations makes analytical approaches intractable. This leaves numerical models as a vital tool for answering many of these lingering questions about Hall thruster physics.

One of the numerical techniques most frequently used to model Hall thruster plasmas is the hybrid-PIC method, in which ions and neutrals are treated using the particle-in-cell (PIC) method and electrons are assumed to behave as a quasi-1D fluid. The first such model, called HPHall,[1] has been the focus of considerable development effort over the past decade. Modifications to the code over this time include the addition and application of an erosion submodel,[2–4] improvements to the wall boundary conditions,[5–8] adjustments to the time-integration and cell-weighting of ions and neutrals,[9] refinement of the electron cross-field mobility model,[6,7,10] and addition of anisotropic differential cross-sections for charge- and momentum-exchange collisions.[11] These efforts resulted in the present version of the code, called HPHall-3.

Despite all these years of development, the collision cross-sections for electron impact ionization — with the exception of single ionization of Xe^{+}[12] — have remained more-or-less unchanged since the code's initial development. Any inaccuracies in the cross-sections for single and double ionization of neutral xenon may result in significant errors in both thruster performance and internal plasma properties. There is also a growing need to include higher charge states such as Xe^{3+} in these numerical models in order to account for the increased quantities of these species at high discharge voltages and in magnetically-shielded thruster

configurations.[13] Hence, the goal of this work consists of two parts: (1) to update the cross-sections for single and double ionization of neutral xenon in HPHall in order to better represent experimental data and (2) to add triply-charged xenon, henceforth referred to as "triple ions" or "triples" for convenience, to the model in order to account for the increased prevalence of this species under modern Hall thruster conditions.

The remainder of this paper is organized as follows: In Section II the technical approach of this work is outlined, including some details of the numerical model and the measurements used for validation. In Section III, simulation results are compared to past work and to experimental measurements. Finally, in Section IV, the findings of this work are summarized and ideas for further development are explored.

II. Technical approach

A. Numerical model overview

HPHall[1] is a numerical model that simulates a Hall thruster discharge using an axisymmetric hybrid-PIC technique. In hybrid-PIC models, the heavy ions and neutrals are treated as macroparticles moving freely within a mesh as with the basic PIC method, whereas electrons are treated as a continuum whose motion is separated into components parallel and perpendicular to magnetic field lines. The plasma is assumed to be quasi-neutral throughout the simulation domain, and the plasma density is computed from the total charge density of ions in the PIC submodel. The plasma potential is computed in the electron submodel using the well-known thermalized potential approximation, found by considering momentum conservation along magnetic field lines:

$$\phi^*(\lambda) = \phi - \frac{k_B T_e(\lambda)}{e} \ln\left(\frac{n_e}{n_{e,0}}\right) \tag{1}$$

where ϕ^* and T_e are constant along magnetic field lines. The thermalized potential ϕ^* is found by momentum conservation across magnetic field lines and the electron temperature T_e is computed via energy conservation across field lines (details in Ref. 1). The magnetic field induced by the plasma is assumed to be negligible compared to the field imposed by the magnetic circuit, which is included as an input to the model. Integration of the governing equations for the electrons and for the heavy species is performed on separate time scales for each, with the electron time step being many times smaller than the ion and neutral time step.

B. Electron mobility

A principal characteristic of HPHall and other hybrid-PIC models is the treatment of electron mobility across magnetic field lines. In a collisionless plasma, the motion of charges along magnetic field lines is unrestricted, whereas motion across field lines is constrained to circular trajectories centered about those lines. In a collisional plasma, the occasional collisions between two particles or between particles and surfaces can cause the guiding center of a charged particle's gyromotion to shift in space, effectively moving the charge across magnetic field lines. However, such a classical analysis of the cross-field mobility of electrons fails to account for the large electron currents observed in Hall thrusters, often called the anomalous electron current or anomalous electron drift. To account for the anomalous electron current, HPHall relies on a semi-empirical correction to the electron collision frequency. In general, the cross-field mobility of electrons can be evaluated as:

$$\mu_{e,\perp} = \frac{e}{m_e \nu_e} \frac{1}{1+\Omega_e^2} \approx \frac{m_e \nu_e}{eB^2} \tag{2}$$

for large values of Ω_e, as is the case in Hall thrusters. The total effective collision frequency ν_e can be written as:

$$\nu_e = \nu_{ei} + \nu_{en} + \nu_w + \nu_b \tag{3}$$

where the effects of electron–electron scattering collisions are neglected. The anomalous Bohm collision frequency ν_b is given by

Downloaded by University of Michigan - Duderstadt Center on December 13, 2017 | http://arc.aiaa.org | DOI: 10.2514/6.2014-3429

$$\nu_b = \alpha \frac{1}{16} \frac{eB}{m_e}. \tag{4}$$

Here, α is a user-defined coefficient that determines the degree to which the anomalous diffusion term influences electron motion. Setting $\alpha = 0$ results in classical cross-field diffusion. In HPHall-3, the Bohm diffusion coefficient α is defined independently in three regions of the thruster discharge:[10] the near-anode or discharge channel region, denoted by the letter c; the thruster exit region, denoted by the letter e; and the plume region, denoted by the letter p. At the boundary between Bohm regions is a buffer zone in which the value of α is interpolated linearly between the values in the neighboring Bohm regions.

As with the α values themselves, the exact location of each Bohm region is defined by the user. Since there are no *a priori* means of determining the regions' appropriate locations or the correct values of the Bohm coefficients, the user must adjust these variables until the simulation results reach an acceptable level of agreement with experimental data. In a previous work on using HPHall to model NASA's HiVHAc EDU2 thruster,[14] this was accomplished by first setting the α values to those found for the H6 6 kW Hall thruster.[10] Then, the location of each of the three discharge regions was adjusted to roughly match the measured discharge current for the thruster operating point being simulated. The plume coefficient α_p was then fixed at 10 and the other two α values were adjusted to better match the discharge current to within a few percent. As a continuation of that work, this work uses the α values and discharge region locations found previously.

C. Ionization collisions

In Hall thrusters, the plasma discharge is ignited and sustained by electron impact ionization of the injected propellant atoms. If the propellant is xenon and only singly- and doubly-charged ions (sometimes referred to as "singles" and "doubles") exist in the plasma, then there are three electron impact ionization reactions to consider:

$$\mathrm{e^- + Xe \rightarrow 2e^- + Xe^+}, \quad \mathrm{e^- + Xe \rightarrow 3e^- + Xe^{2+}}, \quad \mathrm{e^- + Xe^+ \rightarrow 2e^- + Xe^{2+}}. \tag{5}$$

These reactions are also referred to as 0→I, 0→II, and I→II ionization, respectively. From classical kinetic theory, the production rate of single and double ions due to these reactions can be written as

$$\begin{aligned} \dot{n}_i^+ &= n_e n_n \zeta^{0\rightarrow \mathrm{I}}, \\ \dot{n}_i^{2+} &= n_e n_n \zeta^{0\rightarrow \mathrm{II}} + n_e n_i^+ \zeta^{\mathrm{I}\rightarrow \mathrm{II}}. \end{aligned} \tag{6}$$

Since electrons typically have much greater velocities than the heavy species, the rate coefficient ζ for a given reaction can be computed as

$$\zeta = \int_{\epsilon_i}^{\infty} \left(\frac{2\epsilon_e}{m_e}\right)^{1/2} \sigma_i\left(\epsilon_e\right) f_e\left(\epsilon_e\right) d\epsilon_e. \tag{7}$$

Finally, if the electrons follow a Maxwell-Boltzmann energy distribution, then $\zeta = \zeta\left(T_e\right)$. Collision cross-sections can be measured experimentally and a curve fit can then be applied to those data, allowing Eq. (7) to be integrated numerically. In the first version of HPHall, the collision cross-sections for 0→I and 0 →II ionization reactions were based on Drawin curve fits[15] to the data of Mathur and Badrinathan.[16] The Drawin form is given by

$$\sigma_i\left(u\right) = 2.66\pi a_0^2 \xi \beta_1 \left(\frac{\epsilon_i^H}{\epsilon_i}\right)^2 \frac{u-1}{u^2} \ln\left(1.25\beta_2 u\right), \quad u = \frac{\epsilon_e}{\epsilon_i} \tag{8}$$

where β_1 and β_2 are fitting coefficients. Substituting this and a Maxwellian EEDF into Eq. (7) gives

$$\zeta\left(T_e\right) = Q\beta_1 \theta^{-3/2} \int_1^{\infty} \exp\left(-\frac{u}{\theta}\right) \left(\frac{u-1}{u}\right) \ln\left(1.25\beta_2 u\right) du, \quad \theta = \frac{k_B T_e}{\epsilon_i} \tag{9}$$

Downloaded by University of Michigan - Duderstadt Center on December 13, 2017 | http://arc.aiaa.org | DOI: 10.2514/6.2014-3429

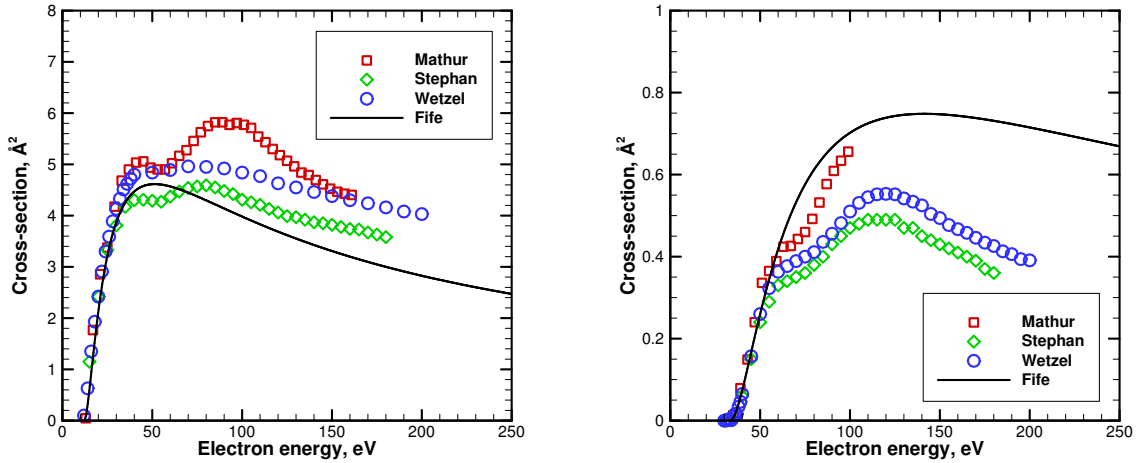

Figure 1: Existing ionization cross-sections in HPHall compared to experimental data for (a) 0→I and (b) 0→II reactions.

where Q is a constant given by

$$Q = 10.64 a_0^2 \left(\frac{\pi k_B \epsilon_i}{2 m_e}\right)^{1/2} \left(\frac{\epsilon_i^H}{\epsilon_i}\right)^2 \xi. \tag{10}$$

In a work by Katz *et al.*[12] the cross-sections for I→II reactions were changed to follow a different form, so this reaction is not considered further here. As reported in Ref. 1, values of $\beta_1 = 1.0$ and $\beta_2 = 0.8$ were used for the 0→I and 0→II ionization reactions in the first version of HPHall. $Q^{0\to\mathrm{I}}$ is reported as $4.13 \times 10^{-13}\,\mathrm{m^3/s}$, corresonding to $\epsilon_i = 12.1$ eV and $\xi = 6$. The value for $Q^{0\to\mathrm{II}}$ is not explicitly given, although it is suggested that $Q^{0\to\mathrm{II}}$ be computed using $\epsilon_i = 33.3$ eV and $\xi = 3$. However, as of the start of this work a value of $Q^{0\to\mathrm{II}} = 1.11 \times 10^{-13}\ \mathrm{m^3/s}$, which corresponds to $\epsilon_i = 33.3$ eV and $\xi = 7.37$, is included in the source code. This value for $\xi^{0\to\mathrm{II}}$ makes little physical sense and is inconsistent with the information given in Ref. 1, so the authors suspect that $Q^{0\to\mathrm{II}}$ was changed in a later version of HPHall in order to better represent the experimental data.

Figure 1 shows the 0→I and 0→II ionization cross-sections implemented in HPHall as of the start of this work alongside experimental measurements from Mathur and Badrinathan,[16] Stephan and Mark,[17] and Wetzel *et al.*[18] Here it is seen that the cross-sections used for 0→I ionization tend to underestimate the measured cross-sections for electron energies greater than 60 eV. The cross-sections for double ionization follow Mathur's measurements reasonably well over the range of those data, but are much greater than the other measurements at high electron energies. In the interest of improving the code's accuracy at the high electron temperatures associated with high discharge voltages and magnetically-shielded thruster configurations, it is necessary to modify these cross-sections to better recreate the existing experimental data.

As a first step towards revising the existing ionization cross-sections, the Drawin curve fits to the experimental data are recomputed. Rather than considering only the data of Mathur and Badrinathan, these curves are fit to all three data sets given in Fig. 1. All curve fits are calculated using a commercial nonlinear least-squares solver. The recomputed cross-sections are shown in Fig. 2 alongside the experimental data and another set of curve fits using a revised Drawin form:

$$\sigma_i(u) = 2.66\pi a_0^2 \xi \beta_1 \left(\frac{\epsilon_i^H}{\epsilon_i}\right)^2 \frac{u-1}{u^{\beta_3}} \ln(1.25\beta_2 u), \quad u = \frac{\epsilon_e}{\epsilon_i}. \tag{11}$$

The coefficients for both the Drawin and revised Drawin fits are given in Table 1. It should be noted that $Q^{0\to\mathrm{II}}$ is computed using $\xi = 6$. Setting $\beta_3 = 2$ in the revised Drawin form recovers Drawin's original function.

Downloaded by University of Michigan - Duderstadt Center on December 13, 2017 | http://arc.aiaa.org | DOI: 10.2514/6.2014-3429

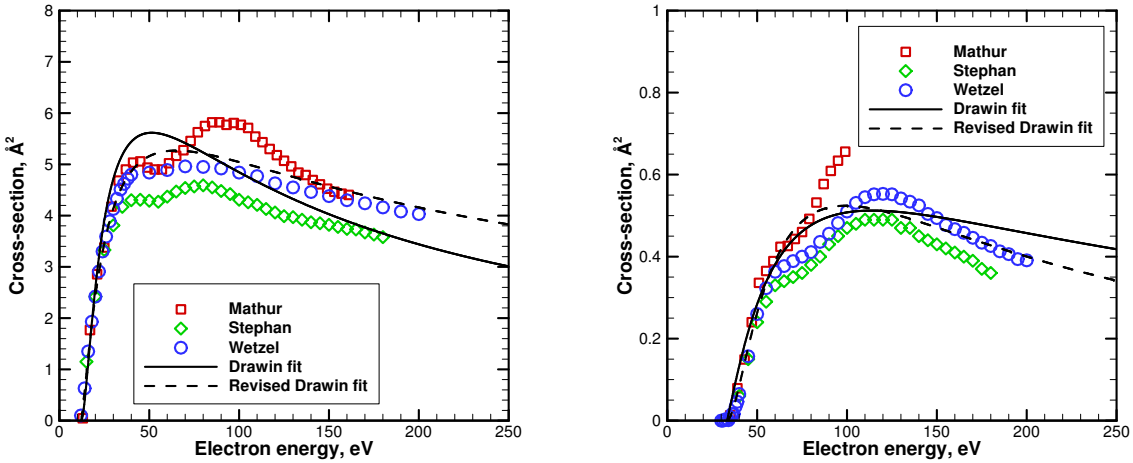

Figure 2: Drawin and revised Drawin fits to experimentally-measured collision cross-sections for (a) 0→I and (b) 0→II reactions.

Table 1: Drawin and revised Drawin fit coefficients for 0→I and 0→II ionization.

Fit		Q, m^3/s	β_1	β_2	β_3
0→I	Drawin	4.13×10^{-13}	1.22	0.8	-
	Revised	4.13×10^{-13}	0.66	1.04	1.74
0→II	Drawin	9.04×10^{-14}	0.62	1.28	-
	Revised	9.04×10^{-14}	1.42	0.87	2.41

The revised Drawin form is motivated by the behavior of the Drawin fits in Fig. 2 at high electron energies. In the case of 0→I ionization, the best-fit Drawin curve seems to decay at a slightly higher rate with increasing electron energy compared to the experimental data, whereas the cross-section for 0→II ionization appears to decay too slowly. The exponent β_3 controls the decay rate in the revised Drawin form, allowing the fitted cross-sections to better capture the high-energy behavior of the experimental data. As a result of this change, the RMS difference between the curve fits and the experimental data increased from 17% to 33% for 0→I ionization and decreased from 180% to 24% for 0→II ionization. The increase in the RMS difference for 0→I ionization results from large differences between the fitted and measured cross-sections at near-threshold energies, where the cross-sections are very small. If cross-sections for electron energies less than 1.1 times the ionization energy are excluded, then the RMS difference is about 13% for both curve fits. Since near-threshold electrons only contribute significantly to ionization at very low electron temperatures ($T_e < 5\,\text{eV}$), the error in the cross-sections at those energies is considered acceptable.

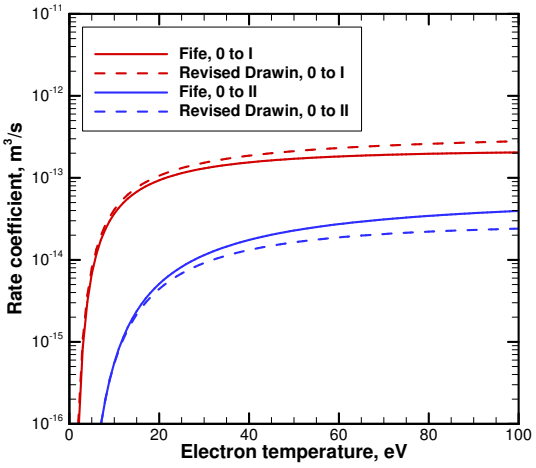

Figure 3: Integrated rate coefficients for 0→I and 0→II ionization reactions.

Downloaded by University of Michigan - Duderstadt Center on December 13, 2017 | http://arc.aiaa.org | DOI: 10.2514/6.2014-3429

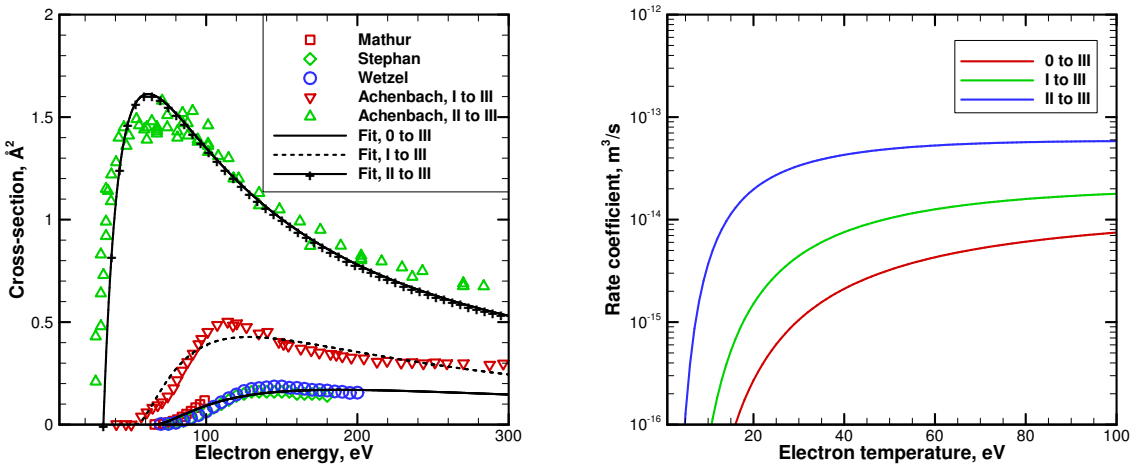

(a) **(b)**

Figure 4: Fitted cross-sections (a) and integrated rate coefficients (b) for 0→III, I→III, and II→III ionization reactions.

Although the revised Drawin form seems to improve the accuracy of the collision cross-sections, it is the integrated rate coefficients that are actually used to compute ionization rates in HPHall-3. The integrated rate coefficients are shown in Fig. 3. For 0→I ionization, the revised Drawin form results in a rate coefficient that is generally greater than that resulting from the existing cross-sections in HPHall. At an electron temperature of 20 eV the rate coefficient is 14% greater, and at 30 eV it is 17% greater. Conversely, for 0→II ionization, the revised fit generally results in a lower rate coefficient, with differences of 13% and 20% at electron temperatures of 20 eV and 30 eV, respectively. However, at an electron temperature of 5 eV, the updated rate coefficient for 0→II ionization is 8% greater than the existing rate coefficient. Hence, an increased rate of double ionization should be expected in low-temperature regions such as the plume, but since the rate of ionization in the plume is already very small this increase should have no effect on performance.

The differences between the existing Drawin ionization rate coefficients and those computed using the revised Drawin fit are only on the order of 10%, but it is expected that they will have a noticeable impact on the Hall thruster simulations. Particularly, since the rate coefficient for single ionization has increased and that for double ionization has decreased, the thruster efficiency predicted by the simulations should increase compared to simulations using the old cross-sections. This is because the momentum carried by an ion of charge state Z is proportional to $Z^{1/2}$, whereas the current carried by the same ion is proportional to $Z^{3/2}$. Hence, increasing the rate of 0→I ionization while decreasing the rate of 0→II ionization should increase the ratio F_{th}^2/I_d, thus increasing the anode efficiency for a given operating point.

D. Triply-charged xenon

Past versions of HPHall have included only single and double ions of xenon. Although triply-charged ions make up no more than a few percent of the total ion current in typical Hall thrusters, the presence of triple ions and even higher-order species becomes more important as discharge voltage increases. There is also evidence to suggest that such high charge states are prevalent in magnetically-shielded Hall thrusters.[13] Hence, modeling high-voltage and magnetically-shielded thrusters using HPHall-3 mandates the addition of these higher charge states, beginning with Xe^{3+}. The three ionization reactions that can result in Xe^{3+} are:

$$e^- + Xe \rightarrow 4e^- + Xe^{3+}, \quad e^- + Xe^+ \rightarrow 3e^- + Xe^{3+}, \quad e^- + Xe^{2+} \rightarrow 2e^- + Xe^{3+}. \tag{12}$$

Of the many changes to the source code required to include triple ions, by far the most significant is the addition of these three ionization reactions. As with the reactions that produce single and double ions, these reactions are modeled using revised Drawin fits to experimentally-measured collision cross-sections.

Downloaded by University of Michigan - Duderstadt Center on December 13, 2017 | http://arc.aiaa.org | DOI: 10.2514/6.2014-3429

The cross-sections for 0→III ionization are based on the data of Mathur,[16] Stephan,[17] and Wetzel.[18] The cross-sections for I→III and II→III ionization are based on the data of Achenbach *et al.*[19,20]

Table 2: Revised Drawin fit coefficients for 0→III, I→III, and II→III ionization reactions.

Fit	ϵ_i, eV	ξ	Q, m^3/s	β_1	β_2	β_3
0→III	65.4	6	3.28×10^{-14}	1.94	0.8	2.48
I→III	53.3	5	3.72×10^{-14}	5.57	0.8	2.85
II→III	32.1	4	6.37×10^{-14}	0.56	1096.5	2.21

The revised Drawin parameters for the three ionization reactions described above are given in Table 2. The cross-sections and the integrated rate coefficients are shown in Fig. 4. As one might expect, the reaction with the highest activation energy (0→III) has the smallest cross-section, whereas the reaction with the lowest activation energy (II→III) has the largest cross-section. This trend translates directly to the rate coefficients, where there is between one and two orders of magnitude difference between the 0→III and II→III reactions. However, since $n_n \approx 10 n_i^+$ and $n_i^+ \approx 10 n_i^{2+}$ in Hall thrusters, each of these reactions may contribute significantly to the population of triple ions.

E. Model validation and simulation setup

The Hall thruster modeled in this work is NASA's HiVHAc EDU2, a product of the High Voltage Hall Accelerator project jointly conducted by NASA Glenn Research Center (GRC) and Aerojet Rocketdyne.[21,22] The goal of the HiVHAc project is to produce a flight-qualified, long-life Hall thruster for use on NASA Discovery-class missions. The EDU2 thruster has demonstrated operation at discharge voltages up to 650 V and discharge powers in excess of 4 kW.[23] The thruster is also highly throttlable, with high-voltage modes approaching 2700 s of I_{sp} and low-voltage modes achieving thrust-to-power ratios competitive with other state-of-the-art Hall thrusters.

Table 3: HiVHAc EDU2 performance as measured in VF-5 for several operating points.

V_d, V	$\dot{m}_a$, mg/s	I_d, A	I_b, A	F_{th}, mN	η_a	p_c, Torr
300.3	10.21	9.96	7.38	186	56.6%	2.7×10^{-6}
400.8	8.29	8.00	6.40	173	56.3%	2.2×10^{-6}
500.0	7.13	6.97	5.58	169	57.5%	1.7×10^{-6}

All performance and plume measurements used for validation were taken in Vacuum Facility 5 (VF-5) at GRC in April–May of 2013. VF-5 is a 18.3 m long, 4.6 m diameter cylindrical vacuum chamber capable of sustaining a no-load background pressure of 1×10^{-7} Torr. The test diagnostics included a Faraday probe swept downstream of the thruster and an inverted pendulum thrust stand. Table 3 summarizes the thruster performance at the three operating points simulated in this work.

In a previous work,[14] HPHall-3 was used to simulate the HiVHAc EDU2 at the operating points given in Table 3. The simulations were performed with a base time step of 5×10^{-8} s and an electron timestep 1000 times smaller. The mesh consisted of 70×30 cells and was generated using a commercial elliptic mesh generator. Simulations on a finer mesh produced similar results, suggesting that the solutions were mesh-independent. The position of the cathode magnetic field line was moved downstream over the course of several simulations until the predicted thrust became constant. Single and double ions and the effects of the background gas were included. Charge exchange collisions were neglected. For each simulation, 20,000

Table 4: HiVHAc EDU2 performance predicted by HPHall-3.

V_d, V	α_c	α_e	α_p	I_d, A	I_b, A	I_b^{2+}, A	F_{th}, mN			η_a
							1	2	3	
300.3	0.18	0.02	10.0	9.85	7.79	1.31	182	175	179	54.8%
400.8	0.2	0.018	10.0	7.99	6.36	1.12	171	164	168	55.1%
500.0	0.09	0.02	10.0	6.94	5.48	1.05	165	157	162	54.8%

Downloaded by University of Michigan - Duderstadt Center on December 13, 2017 | http://arc.aiaa.org | DOI: 10.2514/6.2014-3429

iterations were run without plasma to populate the domain with neutrals. Then, 50,000 iterations were run with the plasma turned on. All data were taken over the last 40,000 iterations to exclude startup oscillations.

The predicted performance parameters from Ref. 14 are reproduced in Table 4. Note that there are three values for thrust. The thrust values reported in Ref. 14 are labeled as $(F_{th})_1$ in Table 4. $(F_{th})_1$ is computed in HPHall-3 as the sum of forces on ions and neutrals plus the electron momentum flux across the cathode magnetic field line. $(F_{th})_2$ is computed as the sum of the neutral, ion, and electron momentum fluxes across the cathode field line, averaged over the course of the simulation. $(F_{th})_3$ is computed as the average momentum flux of ions and neutrals past the downstream mesh boundary. The given efficiency is computed using $(F_{th})_1$.

For all three operating points, the discharge current, ion current, and thrust predicted by HPHall-3 agree with the experimental measurements to within 6%, suggesting that HPHall-3 is capable of accurately simulating HiVHAc EDU2 at voltages of up to 500 V. However, it is expected that the revised cross-sections and the inclusion of triple ions will allow the code to accurately simulate the thruster at even higher discharge voltages.

In this work, simulations are run using the same mesh and base time step as the previous work. However, the ratio $\Delta t_i/\Delta t_e$ is increased from 1000 to 1200 to improve the simulation stability. For simulations including triple ions, the number of ion macroparticles is increased in order to improve stability in the ionization algorithms. Simulations run with twice as many macroparticles overall yield the same results as the baseline simulations, indicating that the results are independent of macroparticle count. Finally, for the purposes of comparing plasma properties, the simulations from the previous work are rerun with one key change: whereas the past work imposed a minimum plasma potential of zero throughout the simulation domain, no such limit is imposed in this work, allowing the minimum plasma potential to arise naturally from the governing equations. This change does not have a significant effect on the computed performance.

III. Results

A. Revised single and double ionization cross-sections

The performance parameters for HiVHAc EDU2 computed using the updated cross-sections are shown in Table 5. The computed efficiencies are based on $(F_{th})_1$. As expected, the predicted efficiency at each operating point is increased as a consequence of the updated cross-sections. The increase in efficiency is associated with an increase in thrust at each operating point with almost no change in the ion current. However, the current carried by double ions decreases relative to the previous work at all three operating points, suggesting the current carried by single ions increases. This is a direct consequence of the rate coefficients shown in Fig. 3. Like the ion current, the discharge current also appears to be unaffected by the change in ionization cross-sections except at 500 V, where it increases by about 1%. Since the ion current is more or less the same at this operating point, the additional discharge current must be carried by electrons.

Table 5: HiVHAc EDU2 performance predicted by HPHall-3 with revised cross-sections for 0→I and 0→II ionization.

V_d, V	I_d, A	I_b, A	I_b^{2+}, A	F_{th}, mN			η_a
				1	2	3	
300.3	9.81	7.82	1.24	184	176	181	56.3%
400.8	8.00	6.35	1.05	173	166	171	56.2%
500.0	7.02	5.50	0.99	168	159	165	56.3%

Figure 5 shows contours of average electron temperature for the 300 V and 500 V operating points with both the old and new ionization cross-sections. For both operating points, the peak electron temperature decreases slightly when the new cross-sections are introduced. At 300 V the peak temperature falls from 22.4 eV to 22.1 eV, and at 500 V it falls from 38.4 eV to 37.5 eV. This suggests that electron energy loss rates are increased in the acceleration zone, where the electron temperature reaches its peak. In the plume, the electron temperature contours appear very similar. This is to be expected since the revised cross-sections are, for the most part, very similar to the old cross-sections at low electron energies.

Figure 6 shows contours of the production rate of single ions, $\dot{n}_i{}^+$. Close investigation of the region of greatest ionization rate shows that the updated cross-sections result in an increased rate of 0→I ionization in that region. This increased rate of 0→I ionization inside the discharge channel is responsible for the

Downloaded by University of Michigan - Duderstadt Center on December 13, 2017 | http://arc.aiaa.org | DOI: 10.2514/6.2014-3429

Downloaded by University of Michigan - Duderstadt Center on December 13, 2017 | http://arc.aiaa.org | DOI: 10.2514/6.2014-3429

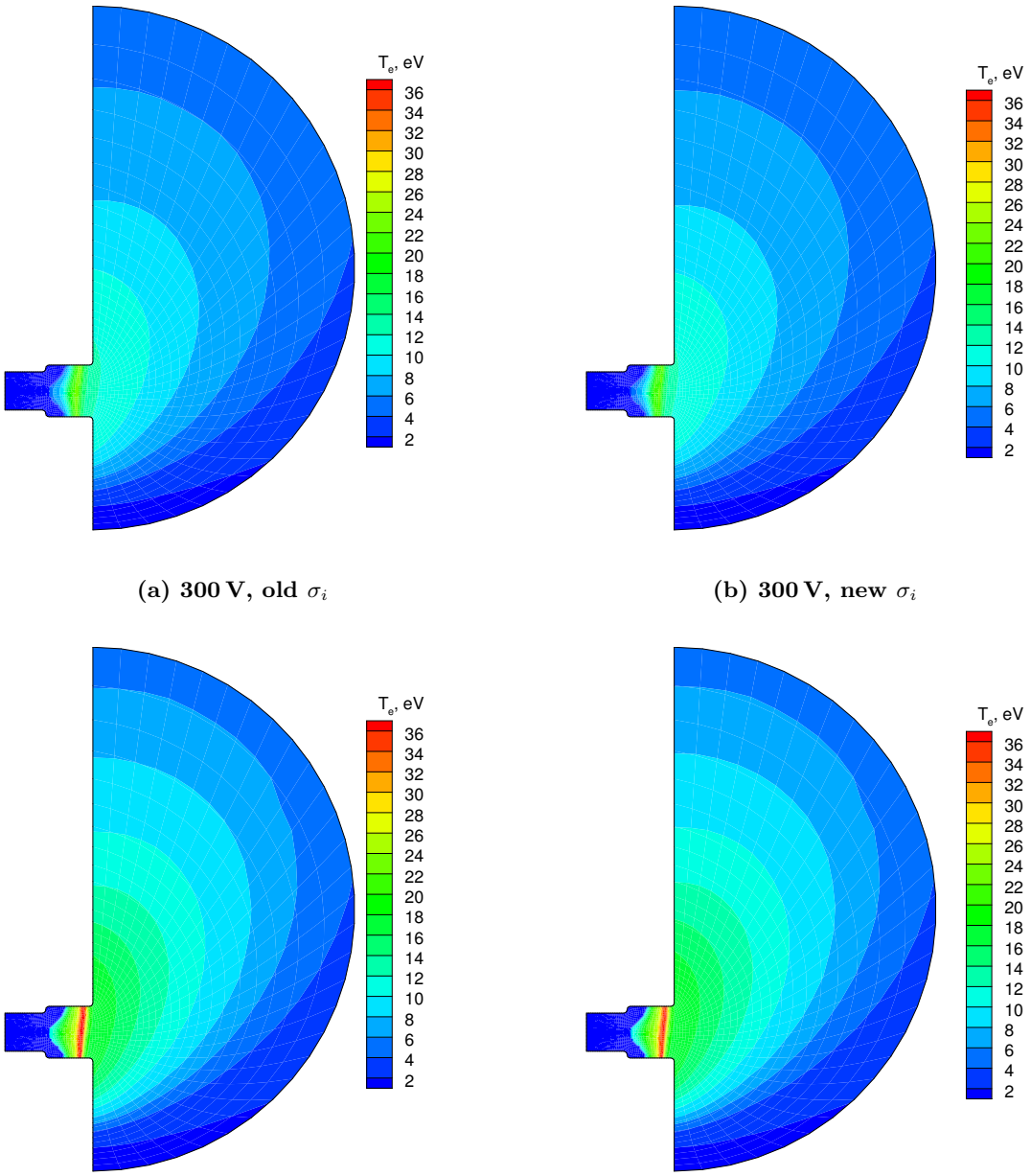

(a) 300 V, old σ_i **(b) 300 V, new σ_i**

(c) 500 V, old σ_i **(d) 500 V, new σ_i**

Figure 5: Contours of electron temperature from HPHall-3 simulations of HiVHAc.

Downloaded by University of Michigan - Duderstadt Center on December 13, 2017 | http://arc.aiaa.org | DOI: 10.2514/6.2014-3429

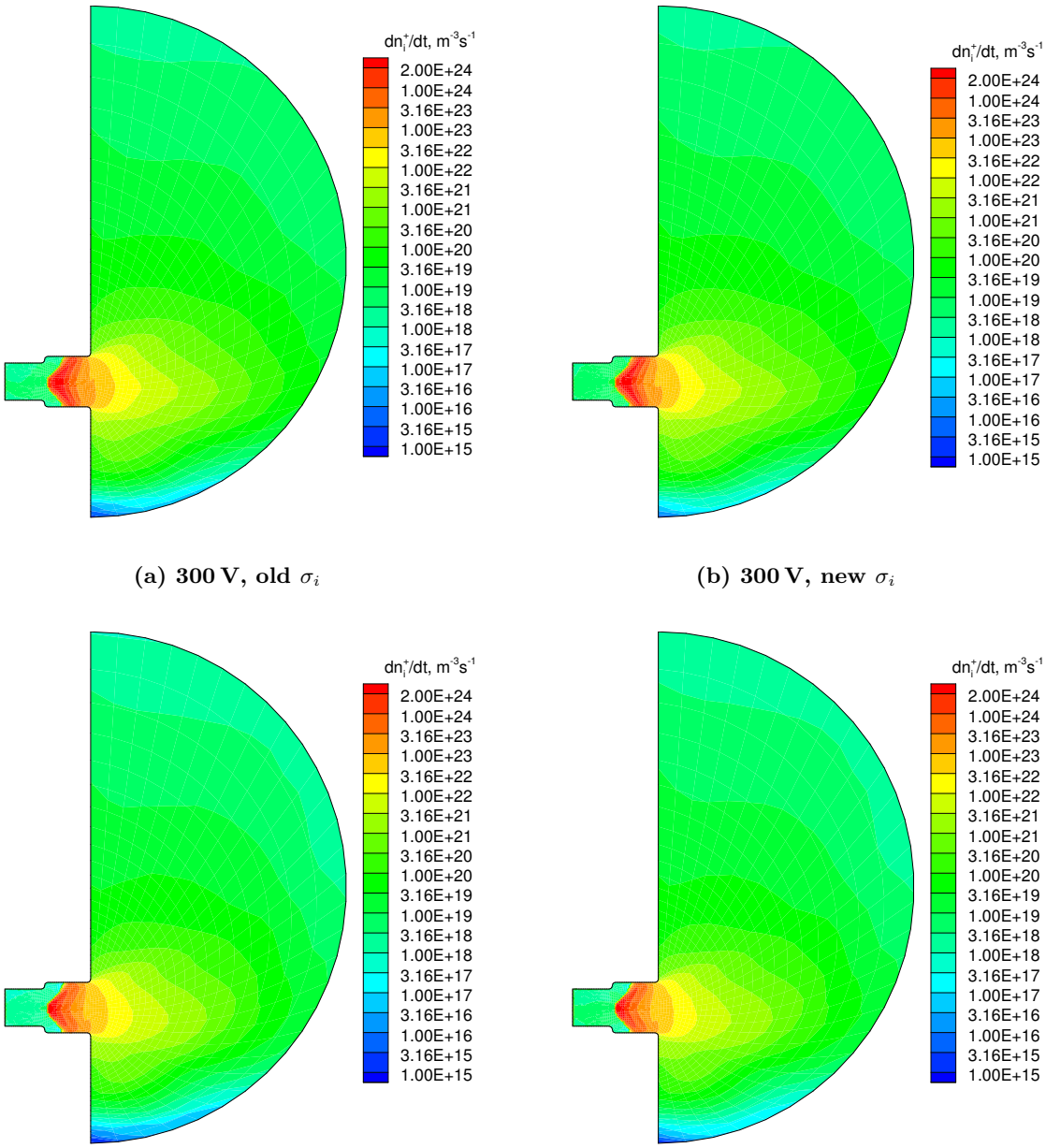

(a) 300 V, old σ_i **(b) 300 V, new σ_i**

(c) 500 V, old σ_i **(d) 500 V, new σ_i**

Figure 6: Contours of 0→I ionization rate from HPHall-3 simulations of HiVHAc.

Downloaded by University of Michigan - Duderstadt Center on December 13, 2017 | http://arc.aiaa.org | DOI: 10.2514/6.2014-3429

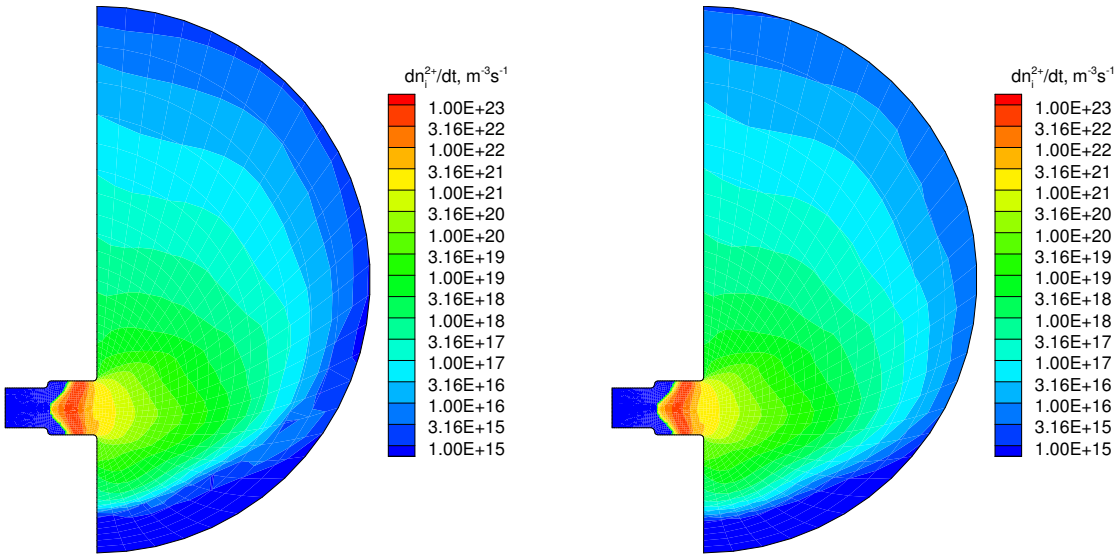

(a) 300 V, old σ_i **(b) 300 V, new σ_i**

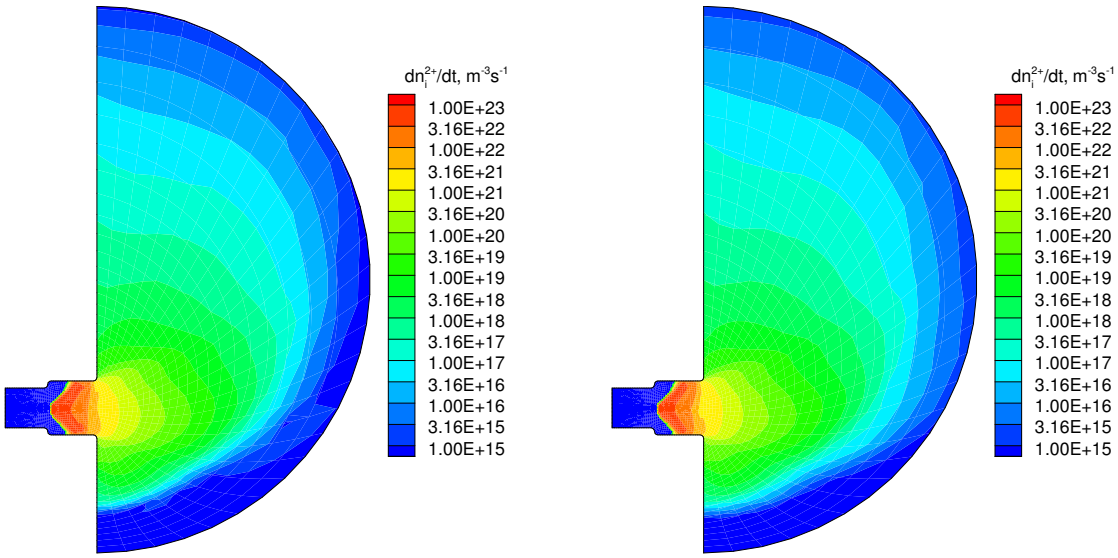

(c) 500 V, old σ_i **(d) 500 V, new σ_i**

Figure 7: Contours of 0→II ionization rate from HPHall-3 simulations of HiVHAc.

reduction in the peak electron temperature. In the plume, however, there is no apparent change in the production rate of single ions, which is consistent with the observed trends in the updated cross-sections at low electron energies.

Figure 7 shows the production rate of double ions due to 0→II ionization reactions. There is a clear decrease in the rate of the 0→II reaction in the ionization region of the discharge channel when the new cross-sections are introduced. The reaction rate in the plume, on the other hand, is increased slightly. This is a consequence of the increase in the 0→II rate coefficient at low electron temperatures. However, since the reaction rate in the plume is very small to begin with, these changes do not seem to affect the predicted thruster performance significantly.

Overall, the introduction of the revised ionization cross-sections appears to have the expected effects on HPHall-3 simulation results. The computed thruster efficiency increases, as predicted, bringing the computed thrust more in line with experimental measurements. The reaction rates and electron temperature follow the expected trends based on the integrated rate coefficients and electron governing equations. Given these observations and the fact that the revised Drawin cross-sections better represent experimental measurements at high electron energies, it can be confidently said that these cross-sections result in an incremental improvement to the accuracy of HPHall-3, especially when high-temperature conditions are present.

Downloaded by University of Michigan - Duderstadt Center on December 13, 2017 | http://arc.aiaa.org | DOI: 10.2514/6.2014-3429

B. Triply-charged ions

Table 6 shows the thruster performance computed by HPHall-3 with the addition of triple ions. Note that all simulations are run with revised Drawin cross-sections for all ionization reactions. The thrust increases slightly at 400 V and 500 V due to the additional momentum carried by the triple ions. The discharge current and ion current also tend to increase. This is a consequence of the $Z^{3/2}$ dependence of the current carried by an individual particle. Indeed, at 400 V and 500 V in particular, the increase in ion current seems to correspond very well to the current carried by triple ions. There is a slight reduction in the current carried by double ions at all operating points, most likely as a consequence of II→III reactions. The fraction of current carried by triple ions tends to increase with discharge voltage, which is expected given that electron temperature also tends to increase with discharge voltage. The anode efficiency increases slightly at 400 V and 500 V operation, which is unexpected given the arguments outlined in Section II. However, since anode efficiency is a derived quantity and is extremely sensitive to other performance parameters, this change is not considered to be significant.

Table 6: HiVHAc EDU2 performance predicted by HPHall-3 including triple ions.

V_d, V	I_d, A	I_b, A	I_b^{2+}, A	I_b^{3+}, A	I_b^{3+}/I_b, A	F_{th}, mN			η_a
						1	2	3	
300.3	9.81	7.84	1.21	0.07	0.8%	184	176	181	56.3%
400.8	8.05	6.40	1.03	0.07	1.0%	174	166	171	56.5%
500.0	7.06	5.57	0.98	0.09	1.6%	169	159	166	56.6%

Based on the performance results, it is unlikely that the electron temperature is significantly affected by the addition of triples. Indeed, as Fig. 8 shows, the electron temperature is virtually unchanged. Since the reaction rates for 0→III, I→III, and II→III tend to be very small, they do not contribute significantly to electron energy losses.

In Section II, it was noted that the production rates of Xe^{3+} due to each of the three associated reactions might be of a similar order of magnitude. In Fig. 9, the triple production rate for each reaction is plotted for 300 V and 500 V operation. Overall, the rate of each of these reactions is at least one order of magnitude smaller than the rate of 0→II ionization, as one might expect. In the discharge channel, it appears as though the rate of each reaction is of similar magnitude, with a reaction rate on the order of $10^{21}\,\mathrm{m^{-3}s^{-1}}$ being typical. In the plume, however, II→III ionization clearly dominates over the other two reactions. The ionization energy for the II→III reaction is much less than that of the other two reactions, and since the electron temperature in the plume is much smaller than in the discharge chamber, there are few electrons that are energetic enough to initiate 0→III or I→III ionization events.

Overall, the trends observed in the simulation results above are consistent with expectations based on the

Downloaded by University of Michigan - Duderstadt Center on December 13, 2017 | http://arc.aiaa.org | DOI: 10.2514/6.2014-3429

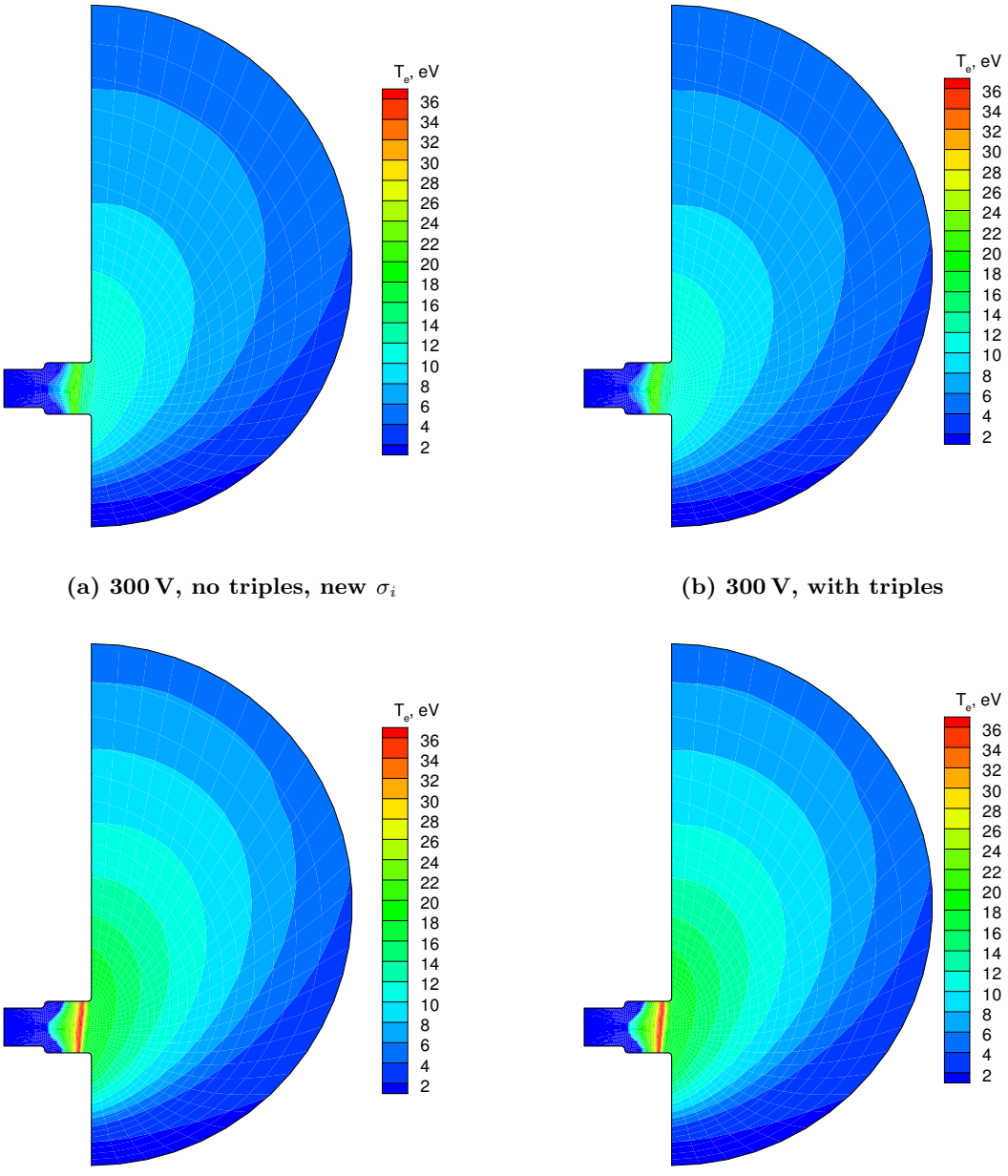

(a) 300 V, no triples, new σ_i **(b) 300 V, with triples**

(c) 500 V, no triples, new σ_i **(d) 500 V, with triples**

Figure 8: Contours of electron temperature from HPHall-3 simulations of HiVHAc after addition of triply-charged ions.

Downloaded by University of Michigan - Duderstadt Center on December 13, 2017 | http://arc.aiaa.org | DOI: 10.2514/6.2014-3429

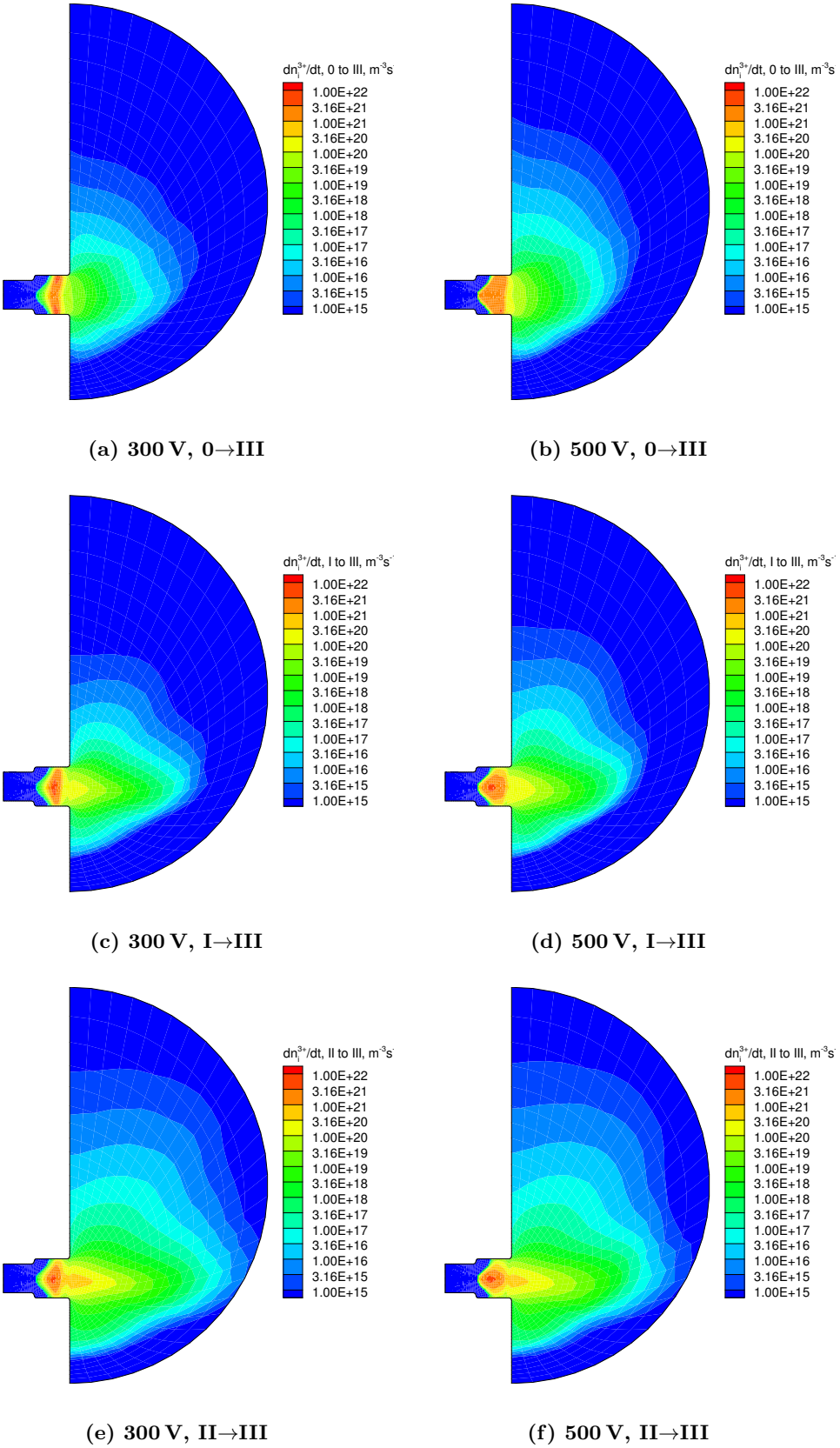

(a) 300 V, 0→III **(b) 500 V, 0→III**

(c) 300 V, I→III **(d) 500 V, I→III**

(e) 300 V, II→III **(f) 500 V, II→III**

Figure 9: Contours of production rate of Xe^{3+} in HiVHAc computed by HPHall-3.

plasma properties found in previous simulations of the HiVHAc thruster using HPHall-3. The effects of triple ions on the simulation results are subtle for the thruster operating points tested herein, but it is expected that triple ions will play a much greater role at higher discharge voltages and in magnetically-shielded Hall thruster configurations, where electron temperatures are typically greater.

IV. Conclusions and future work

In this work, the existing ionization cross-sections in the hybrid-PIC model HPHall-3 have been examined. The existing cross-sections for 0→I and 0→II ionization were found to agree poorly with the experimental data at high electron energies. A revised curve fit based on the Drawin form was proposed and fit to the experimental data, resulting in much better representation of the cross-sections at high electron energies. HPHall-3 simulations of NASA's HiVHAc EDU2 Hall thruster using the revised cross-sections showed an increase in the computed thrust and efficiency, improving the agreement with measured values. The internal plasma properties, namely electron temperature and ionization rates, follow the expected trends based on the changes in the integrated rate coefficients.

The effects of triple ions on HPHall-3 were also investigated. Using the revised Drawin form, curve fits to experimental measurements of 0→III, I→III, and II→III ionization cross-sections were implemented into HPHall-3. Other aspects of the code were updated to include triply-charged ions in the calculations. The simulations of the HiVHAc thruster were repeated with triple ions included, and the predicted thruster performance was shown to change only slightly with the introduction of triples at discharge voltages up to 500 V. Electron temperature contours also appeared to be insensitive to the presence of triple ions. The current fraction carried by triple ions was shown to increase with discharge voltage, as anticipated. The reaction rates for all three triple-producing reactions were found to be of similar order of magnitude in the thruster discharge channel and were all at least one order of magnitude smaller than the rate of 0→II ionization in the previous simulations.

Although the improvements to HPHall-3 presented in this work appear incremental at the operating points examined, it is likely that simulations at other operating points and thruster configurations will show much greater benefit from these changes. For instance, higher discharge voltages tend to result in higher electron temperatures, and hence larger populations of high-energy electrons. State-of-the-art magnetically-shielded Hall thrusters also exhibit increased electron temperatures compared to unshielded configurations, largely as a result of decreased energy losses to the channel walls. Correctly modeling ionization rates due to such high-energy electrons for all relevant ionization reactions is thus critical for modeling high-voltage thrusters. Testing the updated code under such high-temperature conditions is the next step for this work.

Acknowledgments

The research described in this paper was supported with the funding of a NASA Space Technology Research Fellowship, grant #NNX11AM64H.

References

[1]Fife, J., *Hybrid-PIC Modeling and Electrostatic Probe Survey of Hall Thrusters*, Ph.D. thesis, Massachusetts Institute of Technology, 1999.

[2]Gamero-Castaño, M. and Katz, I., "Estimation of Hall Thruster Erosion Using HPHall," *29th International Electric Propulsion Conference*, No. 2005-303, Princeton, New Jersey, USA, Oct. 2005.

[3]Hofer, R. R., Mikellides, I. G., Katz, I., and Goebel, D. M., "BPT-4000 Hall thruster discharge chamber erosion model comparison with qualification life test data," *30th International Electric Propulsion Conference*, Florence, Italy, 2007.

[4]Cheng, S., *Modeling of Hall thruster lifetime and erosion mechanisms*, Ph.D. thesis, Massachusetts Institute of Technology, 2007.

[5]Parra, F. I., Ahedo, E., Fife, J. M., and Martinez-Sanchez, M., "A two-dimensional hybrid model of the Hall thruster discharge," *Journal of Applied Physics*, Vol. 100, No. 2, 2006.

[6]Hofer, R. R., Katz, I., Mikellides, I., and Gamero-Castaño, M., "Heavy Particle Velocity and Electron Mobility Modeling in Hybrid-PIC Hall Thruster Simulations," *42nd AIAA/ASME/SAE/ASEE Joint Propulsion Conference & Exhibit*, No. 2006-4658, Sacramento, California, USA, July 2006.

[7]Hofer, R. R., Mikellides, I., Katz, I., and Goebel, D., "Wall sheath and electron mobility modeling in hybrid-PIC Hall thruster simulations," *43rd AIAA/ASME/SAE/ASEE Joint Propulsion Conference & Exhibit*, No. 2007-5267, Cincinnati, Ohio, USA, 2007.

Downloaded by University of Michigan - Duderstadt Center on December 13, 2017 | http://arc.aiaa.org | DOI: 10.2514/6.2014-3429

[8]Ahedo, E., Santos, R., and Parra, F. I., "Fulfillment of the kinetic Bohm criterion in a quasineutral particle-in-cell model," *Physics of Plasmas*, Vol. 17, No. 7, 2010, pp. 073507.

[9]Parra, F., Escobar, D., and Ahedo, E., "Improvements on particle accuracy in a Hall thruster hybrid code," *42nd AIAA/ASME/SAE/ASEE Joint Propulsion Conference & Exhibit*, No. 2006-4830, Sacramento, California, USA, July 2006.

[10]Hofer, R. R., Katz, I., Mikellides, I., Goebel, D. M., Jameson, K. K., Sullivan, R. M., and Johnson, L. K., "Efficacy of Electron Mobility Models in Hybrid-PIC Hall Thruster Simulations," *44th AIAA/ASME/SAE/ASEE Joint Propulsion Conference & Exhibit*, No. 2008-4924, Hartford, Connecticut, USA, July 2008.

[11]Huismann, T., *Improving Hall Thruster Plume Simulation through Refined Characterization of Near-field Plasma Properties*, Ph.D. thesis, University of Michigan, 2011.

[12]Katz, I., Hofer, R. R., and Goebel, D. M., "Ion Current in Hall Thrusters," *IEEE Transactions on Plasma Science*, Vol. 36, No. 5, Oct. 2008, pp. 2015–2024.

[13]Hofer, R., Goebel, D., Mikellides, I., and Katz, I., "Design of a laboratory Hall thruster with magnetically shielded channel walls, phase II: experiments," *48th AIAA/ASME/SAE/ASEE Joint Propulsion Conference & Exhibit*, No. 2012-3788, Atlanta, Georgia, USA, Aug. 2012.

[14]Smith, B. D., Boyd, I. D., Kamhawi, H., and Huang, W., "Hybrid-PIC modeling of a high-voltage, high-specific-impulse Hall thruster," *49th AIAA/ASME/SAE/ASEE Joint Propulsion Conference & Exhibit*, San Jose, California, USA, July 2013.

[15]Drawin, H.-W., "Zur formelmäßigen Darstellung der Ionisierungsquerschnitte gegenüber Elektronenstoß," *Zeitschrift für Physik*, Vol. 164, 1961, pp. 513–521, in German.

[16]Mathur, D. and Badrinathan, C., "Ionization of xenon by electrons: Partial cross sections for single, double, and triple ionization," *Physical Review A*, Vol. 35, No. 3, 1987, pp. 1033–1042.

[17]Stephan, K. and Mark, T. D., "Absolute partial electron impact ionization cross sections of Xe from threshold up to 180 eV," *The Journal of Chemical Physics*, Vol. 81, No. 7, 1984, pp. 3116–3117.

[18]Wetzel, R., Baiocchi, F., Hayes, T., and Freund, R., "Absolute cross sections for electron-impact ionization of the rare-gas atoms by the fast-neutral-beam method," *Physical Review A*, Vol. 35, No. 2, 1987, pp. 559–577.

[19]Achenbach, C., Mueller, A., Salzborn, E., and Becker, R., "Electron-impact double ionization of I1+ and Xeq+ (q=1,...,4) ions: role of 4d electrons like in photoionization," *Physical Review Letters*, Vol. 50, No. 26, June 1983, pp. 4–7.

[20]Achenbach, C., Mueller, A., Salzborn, E., and Becker, R., "Single ionisation of multiply charged xenon ions by electron impact," *Journal of Physics B: Atomic and Molecular Physics*, Vol. 17, No. 7, 1984, pp. 1405–1425.

[21]Kamhawi, H., Manzella, D., Pinero, L., Haag, T., Mathers, A., and Liles, H., "In-Space Propulsion High Voltage Hall Accelerator Development Project Overview," *45th AIAA/ASME/SAE/ASEE Joint Propulsion Conference & Exhibit*, No. 2009-5282, Denver, Colorado, USA, Aug. 2009.

[22]Kamhawi, H., Manzella, D., Pinero, L., Haag, T., and Huang, W., "In-Space Propulsion High Voltage Hall Accelerator Development Project Overview," *46th AIAA/ASME/SAE/ASEE Joint Propulsion Conference & Exhibit*, No. 2010-6860, Nashville, Tennessee, USA, July 2010.

[23]Kamhawi, H., Haag, T., Huang, W., Shastry, R., Pinero, L., Peterson, T., and Mathers, A., "Performance and Environmental Test Results of the High Voltage Hall Accelerator Engineering Development Unit," *48th AIAA/ASME/SAE/ASEE Joint Propulsion Conference & Exhibit*, No. 2012-3854, Atlanta, Georgia, USA, July 2012.

Downloaded by University of Michigan - Duderstadt Center on December 13, 2017 | http://arc.aiaa.org | DOI: 10.2514/6.2014-3429